Journal Pre-proof

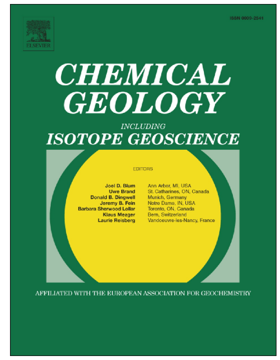

Seawater temperatures during the early to middle Ediacaran: Phosphate oxygen isotope records

Haifeng Fan, Zhigang Chen, Fang Zhang, Chuanwei Zhu, Shengjiang Du, Yuxu Zhang, Hanjie Wen, Danish Khan, Thomas J. Algeo

PII: S0009-2541(25)00032-4

DOI: https://doi.org/10.1016/j.chemgeo.2025.122642

Reference: CHEMGE 122642

To appear in: *Chemical Geology*

Received date: 28 October 2024

Revised date: 18 January 2025

Accepted date: 21 January 2025

Please cite this article as: H. Fan, Z. Chen, F. Zhang, et al., Seawater temperatures during the early to middle Ediacaran: Phosphate oxygen isotope records, *Chemical Geology* (2024), https://doi.org/10.1016/j.chemgeo.2025.122642

Seawater temperatures during the early to middle Ediacaran: phosphate oxygen isotope records

Haifeng Fan[1, 2*], Zhigang Chen[3], Fang Zhang[1, 2], Chuanwei Zhu[1, 2], Shengjiang Du[4], Yuxu Zhang[1, 2], Hanjie Wen[2, 5], Danish Khan[1, 2], Thomas J. Algeo[6,7,8]

1. State Key Laboratory of Ore Deposit Geochemistry, Institute of Geochemistry, Chinese Academy of Sciences, Guiyang 550002, China
2. University of Chinese Academy of Sciences, Beijing 100049, China
3. College of Ocean and Earth Sciences, Xiamen University, Xiamen, 361102, China
4. School of Mining Engineering, Guizhou Institute of Technology, Guiyang 550003, China
5. School of Earth Sciences and Resources, Chang'an University, Xi'an 710054, China
6. Department of Geosciences, University of Cincinnati, Cincinnati, OH 42221-0013, USA
7. State Key Laboratories of Biogeology and Environmental Geology & Geological Processes and Mineral Resources, China University of Geosciences, Wuhan 430074, China
8. State Key Laboratory of Oil and Gas Reservoir Geology and Exploitation, Chengdu University of Technology, Chengdu 610059, China

Corresponding author: H.F. FAN (Email: fanhaifeng@mail.gyig.ac.cn)

Abstract

Early multicellular eukaryotes are hypothesized to have first evolved in deep-water (i.e., subphotic) environments with a narrow temperature range and low oxygen levels (pO_2). However, seawater paleotemperature estimates for the Ediacaran Period remain poorly known. To address this issue, we measured the oxygen isotopic compositions of phosphate ($\delta^{18}O_P$) in fine-grained marine siliciclastic sedimentary rocks from two slope sections of the Doushantuo Formation (~635–551 Ma) in the Nanhua Basin, South China. The bulk $\delta^{18}O_P$ values (~19–26 ‰) found in early-middle Ediacaran phosphatic marine shales represent the oldest known records of modern seawater-like $\delta^{18}O_P$ values. These values are inferred to record original seawater signatures and suggest that subtropical surface temperatures had a modern-like range of 15–30 °C. Based on these estimates, we propose that the extreme greenhouse conditions of the earliest Ediacaran following the Marinoan Ice Age were of quite short duration (<~0.1 Myr). Subsequently, the oldest known metazoan fossil assemblage, the Lantian Biota (~602 Ma), thrived in a deep-water environment characterized by low oxygen levels and a relatively cold, narrow temperature range (~7–8 ± 2 °C). In contrast, the slightly younger Weng'an Biota (~587 Ma) inhabited shallower waters with higher oxygen levels and a broader temperature range (16–30 °C). Finally, our evidence shows that the oxygen isotopic composition of phosphate in fine-grained siliciclastic marine sedimentary rocks can

serve as a valuable proxy for reconstructing the temperature of ancient seawater. Such paleotemperature information, combined with oxygen concentration data, is crucial for understanding the origin and evolution of early animal life.

Keywords:

multicellular; eukaryotes; Doushantuo Formation; South China; Lantian Biota; Weng'an Biota

1. **Introduction**

Seawater paleotemperature plays a crucial role in understanding the co-evolution of Earth's climate and ecosystems. However, there is still ongoing debate regarding the magnitude of temperature changes over geological time. Some studies suggest a significant decline in seawater temperature from the Archean (~70 °C) to the present day (~20 °C) (Robert and Chaussidon, 2006), while other studies have proposed a more limited range of seawater temperatures (~26–35 °C) through Earth history (Blake et al., 2010). Despite these differing perspectives, short-term variations in seawater temperature are widely believed to have been key drivers of extinction and origination events throughout the history of life (Bergmann et al., 2022). Seawater temperature, in particular, exerts a bidirectional limiting influence via the oxygen (O_2) demands of aerobic organisms. Within a narrow temperature range, O_2 requirements are minimized, but even slight decreases or increases in temperature by a few degrees Celsius can result in significant increases in O_2 demand, sometimes by tens of micromoles (Boag et al., 2018; Pörtner, 2010).

The early to middle Ediacaran Period (~635–551 Ma) was a pivotal time in the evolution of multicellular eukaryotes, marked by the emergence of several important fossil assemblages. These include the Lantian Biota (602 ± 7 Ma), Weng'an Biota (~587–574 Ma), Avalon Assemblage (~574 Ma), White Sea Assemblage (560–550 Ma), Miaohe Biota (~550 Ma), and Nama Assemblage (<~550 Ma) (Boag et al., 2018; Xiao et al., 2014). During this interval, deep-water (i.e., subphotic) environments were characterized by low oxygen levels or anoxia (i.e., ferruginous or euxinic conditions), whereas shallow-water (i.e., surface-ocean) environments were generally well-oxygenated (Canfield et al., 2008; Li et al., 2010; Sperling et al., 2015). To explain the origin of multicellular eukaryotes in low-O_2 or anoxic deep-water settings, Boag et al. (2018) proposed the 'stenothermal cradle' hypothesis. According to this hypothesis, the cold and stable temperature conditions of these low-O_2 or anoxic Ediacaran deep-ocean habitats provided a favorable environment for the evolution of early life, particularly the Avalon Assemblage (~574 Ma). These authors also suggested that large temperature fluctuations in shallow waters, which deviate from the optimal range for many species, may have reduced organisms' tolerance to low partial pressure of oxygen (pO_2) (Boag et al., 2018). Despite its critical role in controlling the suitability of habitats for early animal evolution, the temperature of Ediacaran seawater remains poorly constrained. For example, silicon isotopic data from cherts suggested a paleotemperature of approximately 30 °C for Ediacaran ocean-surface water (Robert and Chaussidon, 2006). In contrast, clumped isotopes measurements indicated extremely high and potentially unrealistic temperatures, ranging from 38 to 160 °C, during the Shuram Excursion (~574–551 Ma) (Loyd et al., 2015). Additionally, corrected temperature estimates based on clumped isotopes have indicated a wide range of surface seawater temperatures from 0 to 60 °C (Chang et al., 2022). The lack of agreement among reported paleotemperatures severely limits our understanding of the environmental conditions of origin and evolution of Ediacaran animals.

Phosphate oxygen isotopic compositions ($\delta^{18}O_P$) can be used to reconstruct seawater paleotemperatures (Blake et al., 2010). Based on the narrow range of bulk $\delta^{18}O_P$ values (13–15 ‰) observed in the least-altered phosphorites of the Doushantuo Formation in South China, it was inferred that Ediacaran seawater temperatures were ~34–42 °C, based on a seawater oxygen isotopic composition ($\delta^{18}O_{Seawater}$) of –3 ‰ (Ling et al., 2004). However, sediment $\delta^{18}O_P$ can be strongly influenced by the oxygen isotopic composition of the watermass from which phosphate precipitates. Additionally, regeneration of organic phosphorus within the water column or sediment, involving the hydrolysis of P-O bonds, can alter $\delta^{18}O_P$ compositions (Colman et al., 2005; Jaisi and Blake, 2010). In oxic bottom waters, phosphate (PO_4^{3-}) is released from particulate organic matter and subsequently binds to iron oxyhydroxides (forming Fe-oxide-bound P). During microbial reductive dissolution of Fe-oxides, PO_4^{3-} accumulates in the porewater, commonly leading to the precipitation of apatite (Dijkstra et al., 2018). In modern oxic oceans, strong biological utilization and turnover of PO_4^{3-} result in more equilibrated $\delta^{18}O_P$ values (19–26 ‰) in marine dissolved PO_4^{3-} and authigenic phosphate minerals (Colman et al., 2005; Jaisi and Blake, 2010). These values have significantly evolved from the presumed source $\delta^{18}O$ values of 6–8 ‰ found in apatite from igneous rocks (Smith et al., 2021; Sun et al., 2020). In contrast, anoxic bottom-water conditions often lead to reduced burial of PO_4^{3-} relative to organic carbon in sediments. This is primarily due to the absence of Fe-oxide precipitation, reduced sequestration of polyphosphates, and preferential regeneration of phosphorus from decomposing organic matter (Dijkstra et al., 2018). For example, in the anoxic sediments of modern eutrophic lakes, authigenic apatite often exhibits lower $\delta^{18}O_P$ (15.2±0.6‰) than that expected at equilibrium (16-16.7‰). In contrast, Fe- and Al-bound phosphate minerals typically display higher $\delta^{18}O_P$ values (16.8-23.5‰) relative to equilibrium conditions (Joshi et al., 2015; Yuan et al., 2019). This variation arises from differences in phosphate sources and/or oxygen isotopic fractionation during the formation of various phosphate minerals or phases. Similarly, phosphate associated with Fe-oxides in Archean ferruginous cherts has been observed to exhibit $\delta^{18}O_P$ (>19.9 ‰) similar to that of modern seawater, which is higher than that in phosphorites wherein apatite is the dominant mineral phase ($\delta^{18}O_P$ =10–17 ‰) (Shemesh et al., 1983; Smith et al., 2021; Sun et al., 2020). However, no sources with $\delta^{18}O_p$ values in this range (>19.9 ‰) have been identified in the Precambrian. This observation supports the hypothesis that Fe-oxides, particularly in ancient settings, predominantly adsorb phosphate derived from biological sources. This finding signifies the existence of a well-developed phosphorus cycle intimately linked to biological activity on early Earth (Blake et al., 2010). Given these complexities, it is crucial to account for the intricate dynamics of phosphorus cycling in different redox settings when using the $\delta^{18}O_P$ of sediments to reconstruct ancient seawater temperatures accurately. Failure to do so may lead to oversimplified or inaccurate paleotemperature estimates.

Fine-grained siliciclastic sedimentary rocks have been used to constrain oceanic PO_4^{3-} budgets, as they can capture the large-scale geochemical signals of marine continental margin settings (Reinhard et al., 2017). According to marine shale records and model calculations, previous studies have suggested an increase in the size of the deep-water marine PO_4^{3-} reservoir during the Ediacaran (~635–541 Ma), likely due to enhanced remineralization of organic phosphorus by sulfate-reducing bacteria. This process was accompanied by relatively high apatite and Fe- and Al-bound PO_4^{3-} burial on shallow-marine shelves during the late Proterozoic (~800–635 Ma) (Laakso et al., 2020; Reinhard et al., 2017). These studies further proposed that this fundamental shift in the phosphorus cycle may have led to permanent changes in biogeochemical cycling, primary production, and biological diversity by the end of the Ediacaran Period. In this study, we present new $\delta^{18}O_P$ data from fine-grained siliciclastic sedimentary rocks of the Ediacaran Doushantuo Formation (~635–551 Ma). Based on these data, we reconstruct subtropical ocean-surface paleotemperatures and explore their significance for the origination and evolution of Ediacaran metazoan biotas.

2. Geological setting and samples

In South China, the Nanhua Basin began forming around ~820 Ma as a rift basin between the Yangtze and Cathaysia blocks, with the shallow Yangtze Platform located to its northwest. By the early Ediacaran, when the South China Craton was located at a paleolatitude of ~30 °N (**Fig. S1**), the basin contained a redox-stratified ocean with oxic surface and anoxic deep watermasses (Li et al., 2010; Sahoo et al., 2016), in which accumulation of the thick deposits of the Doushantuo Formation commenced (Jiang et al., 2011) (**Fig. 1A**). This formation, which records the appearance of macroscopic animals and significant populations of eukaryotic phytoplankton (Xiao et al., 2014), is typically subdivided into four members in the Yangtze Gorges area (**Fig. 1B**). During the deposition of the Doushantuo Members II and III (~600–560 Ma; n.b., the focus of the present study), the Yangtze Gorges area was located at subtropical latitudes (~23.5 ± 1.8 °N) (**Fig. S1**) (Zhang et al., 2015).

The Doushantuo Formation contains abundant phosphorite deposits, some preserving remarkable fossil lagerstätten, that accumulated in shallow waters on both the proximal and distal margins of a shelf lagoon (Jiang et al., 2011). A notable example from the Weng'an area of central Guizhou Province is the Weng'an Biota (~587–574 Ma), which is characterized by exceptional cellular preservation (Xiao et al., 2014) (**Fig. 1A, B**). In contrast, the anoxic deep-water facies of the Doushantuo Formation accumulated organic-rich fine-grained siliciclastic sediments. Phosphorite deposits are scarce on the margins of the Yangtze Platform, proximal to the Nanhua Basin (Jiang et al., 2011). The Lantian Biota (~602 ± 7 Ma), the oldest known macroscopic fossil assemblage, consisting of morphologically differentiated benthic algae and putative animals (Yuan et al., 2011), was preserved in slope-basinal settings of upper Member II of the Doushantuo Formation in southern Anhui Province (**Fig. 1A, B**). The Miaohe and Wenghui biotas (~560 Ma), which are dominated by large numbers of filamentous and rhizoidal organisms, were preserved in relatively deep-water (basinal), organic-rich shales (Member IV of the Doushantuo Formation) (**Fig. 1A, B**).

Our samples were collected from the Wuhe and Yinjiang sections in Guizhou Province, which are composed of organic-rich shale deposited in slope settings (**Fig. 1A**). The Doushantuo Formation in the Wuhe area has been subdivided into four members that are correlative with those in the Yangtze Gorges area, where mainly euxinic conditions have been inferred (Sahoo et al., 2016). In contrast, our study section was dominated by ferruginous conditions, but three euxinic intervals are present at the bases of Members II and III and within Member IV (Han and Fan, 2015). Additionally, two phosphorus-rich intervals are observed in the middle of Members II and III (**Fig. 1B**). Although the Wuhe section lacks fossil deposits, a previous study proposed correlations with other South China sections containing fossil lagerstätten (Sahoo et al., 2016) (**Fig. 1B**). For example, the Yinjiang section can be stratigraphically correlated with the Wuhe section (Ye et al., 2017), although some uncertainties remain (**Fig. 1B**). While the seawater redox conditions of the Yinjiang section are not well known, the nearby (~50 km distant) Daotuo section in the same region experienced predominantly anoxic conditions (Ye et al., 2017). A single phosphorite layer is also observed in the middle of the present Yinjiang study section (**Fig. 1B**).

3. Methods

3.1. Phosphate oxygen isotopes and organic carbon isotopes

Phosphate from fine-grained siliciclastic sedimentary rocks was extracted with 1 mol/L HNO_3 following the method of O'Neil et al. (1994). The extracted phosphate was purified and finally converted into pure Ag_3PO_4 solid following a method modified from Blake et al. (2010). The main modifications involved using HNO_3 for acidification and N_2 for purging instead of a cationic resin to remove carbonate ions. This change does not affect the results (Jiang et al., 2017). $^{18}O/^{16}O$ measurements were conducted using a Flash HT-IRMS (1112-series-Delta V Advantage, Thermo Fisher) at Xiamen University and the Third Institute of Oceanography, State Oceanic Administration. All oxygen isotopic compositions are reported relative to the Vienna Standard Mean Ocean Water (VSMOW) in per mille variation (‰). In this study, the $\delta^{18}O_P$ value of the reference material NBS120c is 21.6 ± 0.1 ‰ (1σ, n = 4), consistent with previously published values of 21.7–22.6 ‰ (Lécuyer et al., 2013; Pucéat et al., 2010). Further details of the analytical methods are provided in the **Appendix A**. Organic carbon isotopic compositions ($\delta^{13}C_{org}$) were measured using a Thermo Delta V Advantage isotope ratio mass spectrometer at the Institute of Geology and Geophysics, Chinese Academy of Sciences (IGGCAS). The analytical reproducibility of the reference material GBW04407 is within 0.2 ‰.

3.2. Major elements and mineralogy

All original rock samples were fully digested using a four-acid mixture combining HNO_3, HCl, $HClO_4$, and HF to ensure complete dissolution of our samples. The resulting solution was then evaporated to dryness and redissolved in nitric acid (HNO_3)

(2% v/v). Phosphorus (P), calcium (Ca), and aluminum (Al) concentrations in the resulting solution were measured using an Agilent 7500cs quadrupole inductively coupled plasma mass spectrometer (ICP-MS) at ALS Chemex (Guangzhou) Co., Ltd, with reported relative errors of less than 5 %. After removing the carbonate phase using 1-M HCl, the total carbon content in the residual material was determined using an elementar (vario MACRO cube) at IGCAS. This measurement represents the total organic carbon (TOC), with the analytical reproducibility of the in-house urea standards being within <0.5 %. Mineral observations were conducted using a JSM-7800F scanning electron microscope (SEM) equipped with a TEAM Apollo XL energy-dispersive spectrometer (EDS). The distribution of phosphate and associated minerals in a 3×2-cm thin-section was further analyzed and quantified using a TESCAN Integrated Mineral Analyzer (TIMA) at IGCAS.

4. Results

4.1. Mineralogical compositions

The Wuhe samples exhibit a notable abundance of phosphate minerals (**Fig. 2A, B**), with apatite content ranging from 1.39% to 2.75% (**Table S1**). Vivianite concentrations are lower, ranging from 0.47% to 0.71% (**Fig. S2, Table S1**). Quartz is the dominant mineral in these samples, accounting for up to ~8.94 % by weight. Muscovite is also present at a significant concentration of 30.46%, while biotite occurs in moderate amounts. Hematite/magnetite can reach up to 7.46% (**Fig. S2, Table S1**). Similarly, the Yinjiang samples contain phosphate minerals primarily in the form of apatite, with a concentration of 0.61%. Other phosphates, such as vivianite and gorceixite, are found only in trace amounts (< 0.8%) (**Figs. 2C, D; S3**). The mineral assemblage is dominated by quartz and albite, with quartz peaking at 71.65 % (**Table S1**). Muscovite and biotite are present in smaller quantities, while hematite/magnetite and pyrite appear only in trace amounts (**Fig. S3, Table S1**).

4.2. Isotopic and elemental compositions

In the Wuhe section, bulk $\delta^{18}O_P$ values range from approximately 9.6‰ to 25.5‰ (**Fig. 3, Table S2**). The higher $\delta^{18}O_P$ values are comparable to those found in modern lake and marine sediments. $\delta^{13}C_{org}$ values are predominantly within the range of –38.01‰ to –26.70‰, with many samples clustering toward the more negative endmember (**Fig. 3, Table S2**). When these isotopic trends are compared with TOC/P ratios (mol/mol), a notable correlation emerges: higher $\delta^{13}C_{org}$ values (> –30‰) often correspond to lower TOC/P ratios (<10). In contrast, samples with higher TOC/P ratios (e.g., exceeding the Redfield ratio of 106) generally exhibit more negative $\delta^{13}C_{org}$ values (<–34‰) (**Figs. 3 and 4, Table S2**).

The Yinjiang section exhibits ranges of $\delta^{18}O_P$ and $\delta^{13}C_{org}$ values similar to those of the Wuhe section, although their profiles are distinctly different (**Fig. 3, Table S2**). $\delta^{18}O_P$ ranges from 9.3‰ to 26.0 ‰, and $\delta^{13}C_{org}$ mainly from –37.12 ‰ to –28.01 ‰. Similarly to the Wuhe section, the more negative $\delta^{13}C_{org}$ values correlate with higher TOC/P ratios. Samples with $\delta^{13}C_{org}$ values of –30 ‰ to –28 ‰ display the lowest TOC/P ratios (**Figs. 3 and 4, Table S2**).

5. Discussion

5.1. Fe- and Al-phosphate minerals in anoxic deep-water sediments

In the Nanhua Basin, oxic shallow waters were underlain by predominantly ferruginous deep-water environments, with intermittent euxinic conditions developing along the slope and within the intrashelf basin (Li et al., 2010). Oxic conditions are generally favorable for apatite formation (Dijkstra et al., 2018), and shallow-water phosphorites deposited in oxic inner-shelf and shelf-margin regions of the Yangtze Platform contain abundant apatite minerals (Schwid et al., 2020; Yang et al., 2021), which may have served as a significant sink for dissolved PO_4^{3-} in the Nanhua Basin.

Here, we focus on the phosphorous sink in anoxic sediments. Ferruginous deep-water settings are also favorable phosphorus fixation, in which dissolved PO_4^{3-} is primarily sequestered by iron minerals such as ferrihydrite and green rust. Sequestration in the sediment is followed by release of PO_4^{3-} into porewaters or the overlying water column through partial anaerobic decomposition of organic matter and reduction of Fe-oxides. Ultimately, phosphorus can become fixed in the sediment through formation of authigenic ferrous phosphate minerals, such as vivianite (Egger et al., 2015; Lenstra et al., 2018). Recently, Schwid et al. (2020) identified phosphosiderite as a cement in inner-shelf phosphorites of the Yangtze Platform and suggested that it formed through oxidation of vivianite to phosphosiderite at shallow depths. Additionally, ferric and/or ferrous phosphate minerals (comprising up to 50 % of all phosphate) have been identified in slope deposits of the Wuhe section, along with apatite (**Figs. 2A, B and**

S2; Table S1). These observations indicate that ferruginous and/or euxinic deep-water sediments in the Nanhua Basin represented a major phosphorus sink. However, the Fe:P ratios (> 4) in samples from the Wuhe section are higher than the expected stoichiometric Fe:P ratio of vivianite (1.5–3.0), possibly indicating surface coating by Fe-oxides (Dijkstra et al., 2018). Furthermore, these ferric/ferrous phosphate minerals can dissolve in the presence of even trace amounts of sulfide (Vuillemin et al., 2013), as evidenced by the low total P concentrations in the three euxinic intervals identified in the Wuhe section (**Table S2**).

Interestingly, alongside authigenic apatite and ferric/ferrous phosphate, the Al-phosphate mineral gorceixite is observed in the Yinjiang section (**Figs. 2C, D and S3; Table S1**). Dill (2001) suggested that Al-phosphate minerals commonly precipitate near a source of aluminum (e.g., mica and feldspar) or in environments with high concentrations of dissolved PO_4^{3-}, and that they are more stable at moderate pH levels (4.0–6.8). In contrast, redox processes have little influence on the formation of gorceixite due to its negligible iron content (Jerden and Sinha, 2006). Thus, formation of gorceixite helps to retain phosphorus in the sediment, preventing its release under anoxic conditions. The co-occurrence of gorceixite and apatite in the Yinjiang section indicates varied but generally moderate pH conditions in its depositional environment. Al-phosphate minerals have been estimated to account for a significant fraction (up to ~20 %) of the global sink of modern oceanic phosphorus (Rasmussen, 1996), and they may have played a similar role in the Nanhua Basin during the early to middle Ediacaran.

In summary, authigenic Fe- and Al-phosphate minerals in anoxic, organic-rich deep-water shales functioned as burial sinks for dissolved PO_4^{3-} in the Nanhua Basin, although some detrital and residual organic phosphorus may also have contributed to total phosphorus content.

5.2. Weak phosphorus recycling in the Nanhua Basin

The recycling of PO_4^{3-} prior to its fixation as resistant mineral phases (e.g., apatite, and Fe- or Al-phosphates) is largely controlled by oxygen levels in bottom waters. Furthermore, this recycling process can influence the oxygen isotopic composition of phosphate minerals. Therefore, we will assess phosphorus recycling in the Nanhua Basin. Strong PO_4^{3-} recycling, from both degradation of organic matter and reductive dissolution of Fe-oxide particles upon transport into a euxinic facies, is typically indicated by sedimentary total organic carbon-to-phosphorus ratios (TOC/P, mol/mol) that exceed the Redfield ratio (~106) (Algeo and Ingall, 2007). TOC/P ratios as high as ~1000–1800 have been recorded in sediments associated with ancient oceanic anoxic events (OAEs), although TOC/P ratios in euxinic sediments of the modern Black Sea are no higher than ~200 (Papadomanolaki et al., 2022). In contrast, low TOC/P ratios (< 106, sometimes as low as 10) are common in sediments deposited in oxic and ferruginous facies due to strong sequestration of phosphorus as an absorbed species and/or its precipitation in authigenic mineral phases such as apatite or vivianite (Papadomanolaki et al., 2022).

In the Nanhua Basin, TOC/P ratios and organic carbon isotope compositions

($\delta^{13}C_{org}$) show significant negative correlations ($r = -0.75$ and $p < 0.01$ for Yinjiang; $r = -0.65$ and $p < 0.01$ for Wuhe), with higher TOC/P ratios corresponding to more negative $\delta^{13}C_{org}$ values (**Figs. 3 and 4A; Table S2**). Strongly negative $\delta^{13}C_{org}$ values are typically the result of abundant chemoautotrophic or methanotrophic inputs (e.g., Luo et al., 2014), and previous studies of the Doushantuo Formation have attributed its more negative $\delta^{13}C_{org}$ values (< −32 ‰) to such sources, which are typically associated with euxinic conditions in shelf lagoon (e.g., Jiulongwan) and slope sections (e.g., Siduping) (Fang et al., 2019). In this context, the higher TOC/P ratios (> 106) observed in the Wuhe and Yinjiang sections, as well as in other sections of the Doushantuo Formation (**Fig. 4A**), may be indicative of enhanced phosphorus recycling under euxinic conditions, consistent with iron species records (Han and Fan, 2015; Sahoo et al., 2016). However, more than 60 % of Yinjiang samples with highly negative $\delta^{13}C_{org}$ values (< −32‰) show TOC/P ratios (20–90) that are lower than the Redfield ratio. This discrepancy could be attributed to the formation of abundant authigenic gorceixite and/or Fe-phosphate minerals, rather than an indication of oxic conditions. For instance, non-reducible $Al(OH)_3$ and unreducible ferric and ferrous iron minerals can enhance PO_4^{3-} retention and prevent its release, even under euxinic conditions (Hupfer and Lewandowski, 2008).

Large inputs of cyanobacterial and algal biomass typically produce $\delta^{13}C_{org}$ values ranging from −28 ‰ to −25 ‰ in shallow-shelf and deep-slope areas of South China (Fang et al., 2019). Most of these samples show TOC/P ratios of < 10 (**Fig. 4A**), which are consistent with the values observed in modern and ancient oxic and ferruginous sediments (Algeo and Ingall, 2007; Papadomanolaki et al., 2022). Under ferruginous conditions, scavenging and removal of bioavailable PO_4^{3-} from the water column by iron minerals serves as an important sink for dissolved PO_4^{3-}. During this process, higher rates of vivianite formation compared to apatite authigenesis can led to low TOC/P ratios in ferruginous sediments (Papadomanolaki et al., 2022). Most published TOC/P data for the Nanhua Basin, including those of the present study (**Fig. 4A**), are very similar to values observed in the early Neoproterozoic ferruginous basin of Huainan (mostly < 15), but they are markedly different from those found in modern and ancient euxinic basins (> 106) (Guilbaud et al., 2020; Papadomanolaki et al., 2022). These observations suggest that significant PO_4^{3-} scavenging occurred in the ferruginous water column of the Nanhua Basin during the early to middle Ediacaran Period. This process involved substantial incorporation of PO_4^{3-} into sediments, with limited recycling of PO_4^{3-} from organic matter or sediments back into the water column. Consequently, these phosphate minerals are likely to preserve the oxygen isotope composition of phosphate equilibrated with surface seawater.

5.3. Did Doushantuo phosphate oxygen isotopic compositions reach equilibrium?

5.3.1. Assumed modern seawater-like $\delta^{18}O$ values

Culture experiments indicate that oxygen isotope exchange between dissolved PO_4^{3-} and seawater typically reaches equilibrium within several hours to days driven by enzymatic activity or biologically mediated reactions (Blake et al., 1997; Chang et al., 2021). Consequently, most studies have reported equilibrium oxygen isotope fractionation values of ~20‰ to 24‰ between dissolved PO_4^{3-} and modern seawater or lake water, depending on the ambient water temperature (Colman et al., 2005; Jaisi and Blake, 2010; Joshi et al., 2015; Yuan et al., 2019). However, determining whether Doushantuo Formation phosphate oxygen achieved isotopic equilibrium with Ediacaran seawater requires careful evaluation.

The higher $\delta^{18}O_P$ values (19–25 ‰) observed in organic-rich shales from slope sections are comparable to those found in modern lake and marine sediments (**Fig. 3**) and are likely to reflect equilibrated values. For example, the $\delta^{18}O_P$ values of ferric Fe-bound phosphorus (17–20 ‰) and Al-bound phosphorus (18–23 ‰) are commonly higher than those of authigenic apatite (~15 ‰) in eutrophic sediments from Taihu Lake in eastern China and Chesapeake Bay in the U.S. Higher $\delta^{18}O_P$ values recorded in Fe-Al phosphate minerals were explain by terrestrial source (Yuan et al., 2019). However, no sources with $\delta^{18}O_p$ values in this range have been identified during the Precambrian. This consideration supports the hypothesis that Fe- and Al-phosphate, at least in ancient settings, primarily adsorb phosphate derived from biological sources. Although the oxygen isotopic composition of Ediacaran seawater ($\delta^{18}O_W$) is not well constrained, multiple lines of evidence suggest it has remained relatively constant, with a modern seawater-like $\delta^{18}O_W$ value of 0 ± 2 ‰ throughout Earth history (Bergmann et al., 2022; Bergmann et al., 2018). Neither biotic nor abiotic processes are thought to have a significant influence on the oxygen isotopic signatures of Al-phosphate minerals (Yuan et al., 2019). Therefore, the high $\delta^{18}O_P$ values (>19 ‰) observed in the Yinjiang section (**Fig. 3**) may represent the primary equilibrium oxygen isotopic signal of dissolved

PO_4^{3-} in Ediacaran ocean-surface waters, assuming a near-zero $\delta^{18}O_W$ value. Unlike Al-phosphate minerals, ferric Fe-bound phosphate is prone to reductive dissolution under hypoxic and anoxic (euxinic) water columns or sediment conditions. During this process, PO_4^{3-} released from ferric Fe below the redoxcline can undergo enzyme-mediated oxygen isotopic exchange with bottomwater or porewater, which could shift $\delta^{18}O_P$ values depending on the rate of isotopic exchange, which is biologically mediated. Recycled phosphorus can subsequently be trapped by colloidal ferric (oxy)hydroxides or form ferrous phosphate minerals, such as vivianite, near the redoxcline. During this process, coprecipitated or occluded phosphate may preserve the seawater $\delta^{18}O$ value (Jaisi et al., 2011). Notably, phosphate associated with Fe-oxides in Archean anoxic cherts has been shown to record $\delta^{18}O_P$ values (up to 19.9 ‰) reflecting the oxygen isotopic signature of dissolved PO_4^{3-} in ambient seawater (Blake et al., 2010), due to little fractionation between dissolved inorganic phosphate and iron-oxides.

Based on these considerations, the high $\delta^{18}O_P$ values (>19 ‰) observed in the slope Wuhe section, similar to those in the Yinjiang section (20 ± 2 ‰), likely represent the lowest primary oxygen isotopic signal of dissolved PO_4^{3-} in equilibrium with surface seawater, assuming phosphorus was terrestrially sourced. This interpretation is consistent with the oxygen isotopic equilibrium fractionation observed between authigenic phosphate minerals in ancient sediments and porewaters (Jaisi and Blake, 2010). Thus, these $\delta^{18}O_P$ values (> 19 ‰) may be used to estimate the lower limit of ocean-surface temperatures during the Ediacaran Period, although some uncertainties remain due to the limited criteria available for determining equilibrium conditions, the potential for detrital contamination, and the limited constraints on Ediacaran seawater $\delta^{18}O_W$ values.

5.3.2. Assumed non-modern seawater-like $\delta^{18}O$ values

If the $\delta^{18}O_P$ values of ~19–25 ‰ from the two slope sections (**Fig. 4**) represent an equilibrium with Ediacaran ocean-surface $\delta^{18}O$, then other measured $\delta^{18}O_P$ values deviating from this equilibrium (i.e., <19 ‰) must represent different pathways. Several possible explanations exist. First, seasonal local freshwater inputs with lower $\delta^{18}O$ values (–6 to −10 ‰) (Fan et al., 2022) could have decreased the $\delta^{18}O$ of nearshore watermasses on the Yangtze Platform. Recent studies based on elemental salinity proxies have adduced substantial evidence of at least intermittently reduced-salinity conditions in Neoproterozoic seas of South China (Cheng et al., 2021, 2023; Yu et al., 2022; Wei et al., 2024; Liu et al., 2025). Salinity reductions were larger in shallow platform areas compared to deeper basinal areas (Liu et al., 2025) and were broadly enhanced during eustatic lowstands, i.e., when the Nanhua Basin was relatively more isolated from the global ocean by its shallow boundary sills (Cheng et al., 2021).

Second, detrital phosphate minerals are highly insoluble and resistant to depositional, biological, and diagenetic alteration, thus retaining the isotopic signature of igneous phosphate minerals (5.3–7.0 ‰) (Jaisi and Blake, 2010; Ruttenberg and Berner, 1993). The lowest $\delta^{18}O_P$ values (9–12 ‰) observed in our two slope sections are very close to those of volcanic apatite (Smith et al., 2021), suggesting the possible presence of detrital phosphate minerals in fine-grained sediments of the slope sections.

This is supported by the P/Al ratios of a subset of the study samples that have values close to the crustal average (**Table S2**). If this interpretation is correct, a two-component mixing model based on detrital and authigenic phosphate endmembers with $\delta^{18}O_P$ compositions of 6.8 ‰ and ~22 ‰, respectively, requires a ~40–70% contribution from detrital sources.

Third, given that most of the study samples have P/Al ratios higher than the crustal average (**Figs. S2, S3, and S4; Table S2**), mass balance considerations between authigenic apatite and Fe- and Al-phosphate minerals may provide an explanation. Authigenic apatites in modern Taihu Lake, China (15.28 ‰) and Chesapeake Bay, USA (14.5 ‰) typically show $\delta^{18}O_P$ values that are ~3–8 ‰ lower than those of coexisting Fe-Al phosphate minerals (>17–23 ‰). This difference has been attributed to the regeneration of inorganic phosphorus during organic matter degradation (Joshi et al., 2015; Yuan et al., 2019), wherein the $\delta^{18}O_P$ values of freshly regenerated inorganic phosphorus are ~7–12 ‰ lower than calculated equilibrium values (Blake, 1998; Liang and Blake, 2006). $\delta^{18}O_P$ values of phosphorites from the Weng'an section (located ~100 km from Wuhe and ~200 km from Yinjiang) are typically < 18 ‰, with an average value of ~15.5 ‰ (Ling et al., 2004; Yang et al., 2021). In our samples, more than 80 % of those with $\delta^{18}O_P$ values below 19 ‰ also show extremely low TOC/P ratios (**Fig. 4B**), suggesting that authigenic apatite derived from primary mineral P may be influencing $\delta^{18}O_P$. This hypothesis is further supported by our mineral observations: samples with lower $\delta^{18}O_P$ (< 15 ‰) generally contain more apatite, while those with higher $\delta^{18}O_P$ (> 19 ‰) contain more Fe- and Al-phosphate (**Figs. S2 and S3; Tables**

S1 and S2).

A fourth and final possibility is that strong regeneration of organic phosphorus into dissolved inorganic phosphate during early diagenesis can result in nonequilibrium oxygen isotopic signatures of fresh inorganic PO_4^{3-} in the ambient seawater or porewater, which may also be potentially influenced by oxygen isotope exchange with detrital clay minerals (Colman et al., 2005; Joshi et al., 2015; Liang and Blake, 2006) (**Figs. S2 and S4**). This possibility is supported by the relationship between TOC/P ratios, muscovite abundance, and $\delta^{18}O_P$ values, where most samples with TOC/P > 106 and muscovite > 2 % display $\delta^{18}O_P$ values that deviate from modern seawater (Figs. 4B and S5). In this study, $\delta^{18}O_P$ values < 19 ‰ were not used to calculate seawater paleotemperatures due to these uncertainties.

Here, we acknowledge the limitation of our leaching method without extrication specific phosphate phase such as apatite, Fe- and Al-phosphate and over-interpretations (e.g. mass balance calculations), and will develop more suitable extraction method for those ancient sediments.

5.4. Paleoclimate during the early to middle Ediacaran

In this study, surface seawater paleotemperatures were calculated using a phosphate oxygen isotopic equilibrium equation, T(°C) = 117.4(±9.5) – 4.50(±0.43) × ($\delta^{18}O_P$ – $\delta^{18}O_W$) (Lécuyer et al., 2013), adopting an assumed $\delta^{18}O_W$ value of 0 ± 2 ‰ for ice-free global seawater (Bergmann et al., 2022). This preference is based on agreement of the temperatures yielded by this equation with those obtained from coexisting carbonates. The calculated average paleotemperatures are shown in **Fig. 5** and given in **Table S2**.

The Snowball Earth hypothesis suggests an extreme greenhouse climate following the Neoproterozoic Marinoan Ice Age (~651-635 Ma) (Bao et al., 2008; Hoffman et al., 1998). However, our calculated surface seawater average paleotemperatures during deposition of the lower Doushantuo Member II (~630 Ma) are ~0 °C at Yinjiang and ~15 °C at Wuhe (**Fig. 5**). Although there is some uncertainty in the stratigraphic correlation between these two sections, we infer that the extreme greenhouse climate following the Marinoan Glaciation either ended very early during the deposition of the Doushantuo Formation or may not have occurred at all. This interpretation is supported by other studies that challenged the extreme greenhouse hypothesis, suggesting that atmospheric CO_2 pressure may have been as low as the current value of 400 ppm (Sansjofre et al., 2011).

Regardless of the climate scenario, high $^{87}Sr/^{86}Sr$ ratios (~0.708–0.722) demonstrate strong continental weathering at the beginning of Member II (Hohl et al., 2022). This enhanced weathering could have increased the terrestrial phosphorus flux to the global ocean, promoting extensive phosphorite deposition at both inner- and outer-shelf locations. Combined with changes in phosphorus supply due to increased regeneration and upwelling from the open ocean, these factors likely contributed to the formation of phosphogenic environments during the early Ediacaran (Laakso et al., 2020). However, strong phosphorus recycling from organic matter and Fe-oxides was only recorded in the earliest euxinic intervals of the basin sections (Jin et al., 2018) and the Wuhe slope section (this study). This suggests effective PO_4^{3-} scavenging and burial as phosphate minerals, rather than remineralization in the dominantly ferruginous deep waters of the Nanhua Basin.

These findings have implications for contemporaneous oceanic oxygenation and evolution of early metazoans. Enhanced dissolved PO_4^{3-} concentrations in the water column could have stimulated higher primary production, as indicated by the abundance of cyanobacteria and algae (evidenced by $\delta^{13}C_{org}$ values, **Fig. 3**). This increased primary production would have supplied free oxygen that diffused into deep-water habitats, where the Lantian Biota developed. Paleontological evidence suggests increased oxygen availability (Yuan et al., 2011), but geochemical data indicate persistent euxinia with only transient intervals of oxygenation (Wang et al., 2017). During this time, surface seawater temperatures were estimated to be ~13 °C at Wuhe and ~16 °C at Yinjiang, yielding an average estimate of ~14.5 ± 2.1 °C for these two sections (**Fig. 5**). Considering seawater temperature and oxygen availability, the Lantian Biota likely developed in deep-water environments with relatively low oxygen levels and cold, stable temperatures, within a narrow range of ~7–8 ± 2 °C. This is based on the observed decrease in temperature with increasing paleolatitude of ~5 °C per 10° northwards, and a temperature decrease of ~1–2 °C per 100 meters of water depth (Rhein et al., 2013) (see **Appendix A**). These stable temperature conditions could have significantly increased the tolerance of the Lantian Biota to low oxygen levels by modulating oxygen supply and demand.

The lowest seawater temperatures (~4.5 ± 0.7 °C) are recorded in the middle of both study sections (**Fig. 5 and Table S2**). Moreover, the Wuhe section shows a gradual cooling trend, consistent with a recent study that reported a similar paleotemperature trend (based on clumped isotopes) in an inner-shelf section of the Yangtze Platform, which was attributed to the influence of the ~580-Ma Gaskiers Glaciation (Chang et al., 2022). Although Gaskiers glacial sediments have not been documented on the Yangtze Platform, our data provide direct evidence of a gradually cooling climate that may have been a far-field effect of the Gaskiers glaciation (**Fig. 5**). However, precise age constraints are needed to validate this hypothesis.

During a slightly earlier period (~587 Ma), the Weng'an Biota thrived in a shallow-water environment (i.e., within the photic zone and above the fair-weather wavebase) on the outer shelf, suggesting it was preserved in waters with relatively high oxygen levels (Xiao et al., 2014). At that time, estimated surface seawater paleotemperatures as 16–29 °C in the Wuhe section (mostly between 16 °C and 20 °C), and up to ~31 °C in the Yinjiang section (based on a single sample) (**Fig. 5 and Table S2**). Previous studies have suggested that a wide range of temperatures in shallow waters could increase O_2 requirements for the aerobic respiration of metazoans (Boag et al., 2018), which may explain the high O_2 demands of the Weng'an Biota living on the shallow outer shelf.

Following the cooling event, surface seawater paleotemperatures in the Wuhe section gradually increased from 10 °C to 28 °C, while in the Yinjiang section, they abruptly rose to ~30 °C (**Fig. 5 and Table S2**). This large fluctuation in seawater temperature likely disrupted the embryonic development of the Weng'an Biota. Although a complete seawater paleotemperature curve is unavailable, estimates suggest that the surface seawater paleotemperatures at the paleolatitude of 20–24°N (see **Appendix A**) ranged from 15 °C to 30 °C (22 ± 6 °C) throughout most of deposition of the Doushantuo Formation deposition, except during the transient cooling events associated with the Marinoan and Gaskiers glaciations (**Fig. 5**).

Finally, we suggest that the modern seawater-like $\delta^{18}O_P$ values observed in ferruginous marine fine-grained siliciclastic sedimentary rocks were likely a common feature throughout the Precambrian. These values may reflect relatively small variations in seawater paleotemperature, ranging from 26–35 °C during the Archean (Blake et al., 2010) to mostly 15–30 °C during the early to middle Ediacaran Period (this study). Optimal temperatures maximize aerobic scope and require the lowest O_2 levels. However, pO_2 tolerance decreases significantly, and oxygen demands increase by approximately 6 % when the temperature deviates from the optimal value by ~4 °C (Boag et al., 2018). Therefore, constructing a more accurate seawater paleotemperature profile is crucial for understanding the origin and evolution of early life, especially when integrated with the redox conditions of ancient seawater.

6. Conclusions

In this contribution, we propose that, in addition to apatite, Fe- and Al-phosphate minerals (e.g., vivianite, gorceixite) may have served as significant sinks for dissolved phosphorus in anoxic deep-water sediments in the Nanhua Basin during the early to middle Ediacaran Period. This contrasts with the more active phosphorus recycling observed in other coeval basins globally. Phosphate oxygen isotopic compositions from marine fine-grained siliciclastic sedimentary rocks of the Ediacaran Doushantuo Formation show a wide range, from 9.3 ‰ to 26 ‰. Using $\delta^{18}O_P$ values exceeding 19 ‰ (with those lower values likely have been altered) and assuming a near-zero seawater oxygen isotopic composition, we estimated a modern subtropical seawater-like paleotemperature of 22 ± 6 °C. Our newly reconstructed paleotemperatures provide valuable insights into the oxygen requirements and tolerance of Ediacaran multicellular eukaryotes. However, further research is necessary to refine these estimates through extraction of specific phosphate phases to fully understand the implications for early life evolution.

Acknowledgments

This research was funded by the NSFC (92062221, 42121003, 42073016), Guizhou Provincial Science and Technology Subsidies (GZ2020SIG, GZ2021SIG), Project of Guizhou Basic Research Plan-2025 (Natural Science), and Start-up Fund for High-level Talents of Guizhou Institute of Technology (2023GCC048). We also thank Dr. Xinqiang Wang for providing five samples from the Wuhe section.

Appendix A. Supplementary Material. This includes accompanying information to support the study, comprising: 1) Detailed analytical methods for oxygen isotope analysis of phosphate, 2) Seawater paleotemperature estimation for biotas, and 3) TIMA figures illustrating the mineral distribution of phosphate and other associated components.

References

Algeo, T.J., Ingall, E., 2007. Sedimentary C_{org}:P ratios, paleocean ventilation, and Phanerozoic atmospheric pO_2. Palaeogeography, Palaeoclimatology, Palaeoecology 256, 130-155.

Bao, H., Lyons, J.R., Zhou, C., 2008. Triple oxygen isotope evidence for elevated CO_2 levels after a Neoproterozoic glaciation. Nature 453, 504-506.

Bergmann, K.D., Al Balushi, S.A.K., Mackey, T.J., Grotzinger, J.P., Eiler, J.M., 2018. A 600-million-year carbonate clumped-isotope record from the Sultanate of Oman. Journal of Sedimentary Research 88, 960-979.

Bergmann, K.D., Boekelheide, N., Clarke, J.W., Cantine, M.D., Wilcots, J., Anderson, N.T., Jost, A.B., Laub, O., Drozd, J., Goldberg, S.L., Mackey, T., Meyer, F., Eyster, A., 2022. Temperature: a key driver of Earth's habitability over the last billion years. Earth and Space Science Open Archive, 57.

Blake, R.E., 1998. Enzyme-catalyzed oxygen isotope exchange between inorganic phosphate and water: reaction rates and temperature dependence at 5.7-30° C. Mineralogical Magazine, 163-164.

Blake, R.E., O'Neil, J.R., Garcia, G.A., 1997. Oxygen isotope systematics of biologically mediated reactions of phosphate: I. Microbial degradation of organophosphorus compounds. Geochimica et Cosmochimica Acta 61, 4411-4422.

Blake, R.E., Chang, S.J., Lepland, A., 2010. Phosphate oxygen isotopic evidence for a temperate and biologically active Archaean ocean. Nature 464, 1029-1032.

Boag, T.H., Stockey, R.G., Elder, L.E., Hull, P.M., Sperling, E.A., 2018. Oxygen, temperature and the deep-marine stenothermal cradle of Ediacaran evolution. Proceedings of the Royal Society B: Biological Sciences 285, 20181724.

Canfield, D.E., Poulton, S.W., Knoll, A.H., Narbonne, G.M., Ross, G., Goldberg, T., Strauss, H., 2008. Ferruginous conditions dominated later Neoproterozoic deep-water chemistry. Science 321, 949-952.

Chang, B., Li, C., Algeo, T.J., Lyons, T.W., Shi, W., Cheng, M., Luo, G., She, Z., Xie, S., Tong, J., Zhu, M., Huang, J., Foster, I., Tripati, A., 2022. A ~60-Ma-long, high-resolution record of Ediacaran paleotemperature. Science Bulletin 67, 910-913.

Chang, S.J., Blake, R.E., Colman, A.S., 2021. Oxygen isotope exchange rates between phosphate and water catalyzed by inorganic pyrophosphatase: Implications for the biogeochemical cycle of phosphorus. Earth and Planetary Science Letters 570, 117071.

Cheng, M., Zhang, Z., Algeo, T.J., Liu, S., Liu, X., Wang, H., Chang, B., Jin, C., Pan, W., Cao, M., Li, C., 2021. Hydrological controls on marine chemistry in the Cryogenian Nanhua Basin (South China). Earth-Science Reviews 218, 103678.

Cheng, M., Zhang, Z., Jin, C., Wei, W., Wang, H., Algeo, T.J., Li, C., 2023. Salinity variation and hydrographic dynamics in the early Cambrian Nanhua Basin (South China). Science China Earth Sciences 66(6), 1268-1278.

Colman, A.S., Blake, R.E., Karl, D.M., Fogel, M.L., Turekian, K.K., 2005. Marine phosphate oxygen isotopes and organic matter remineralization in the oceans. Proceedings of the National Academy of Sciences (U.S.A.) 102, 13023-13028.

Dijkstra, N., Hagens, M., Egger, M., Slomp, C.P., 2018. Post-depositional formation of vivianite-type minerals alters sediment phosphorus records. Biogeosciences 15, 861-883.

Dill, H.G., 2001. The geology of aluminium phosphates and sulphates of the alunite group minerals: a review. Earth-Science Reviews 53, 35-93.

Egger, M., Jilbert, T., Behrends, T., Rivard, C., Slomp, C.P., 2015. Vivianite is a major sink for phosphorus in methanogenic coastal surface sediments. Geochimica et Cosmochimica Acta 169, 217-235.

Fan, M., Foote, J.M., Martin, A.J., Zhu, L., 2022. Stable isotope compositions of surface water in Mexico between 22–26 °N. Journal of South American Earth Sciences 115, 103723.

Fang, X., Wu, L., Geng, A., Deng, Q., 2019. Formation and evolution of the Ediacaran to Lower Cambrian black shales in the Yangtze Platform, South China. Palaeogeography, Palaeoclimatology, Palaeoecology 527, 87-102.

Guilbaud, R., Poulton, S.W., Thompson, J., Husband, K.F., Zhu, M., Zhou, Y., Shields, G.A., Lenton, T.M., 2020. Phosphorus-limited conditions in the early Neoproterozoic ocean maintained low levels of atmospheric oxygen. Nature Geoscience 13, 296-301.

Han, T., Fan, H., 2015. Dynamic evolution of the Ediacaran ocean across the Doushantuo Formation, South China. Chemical Geology 417, 261-272.

Hoffman, P.F., Kaufman, A.J., Halverson, G.P., Schrag, D.P., 1998. A Neoproterozoic Snowball Earth. Science 281, 1342-1346.

Hohl, S.V., Jiang, S.-Y., Becker, H., Wei, H.-Z., Wei, G.-Y., Xu, J., Guo, Q., Viehmann, S., van Acken, D., 2022. Spatiotemporal evolution of late Neoproterozoic marine environments on the Yangtze Platform (South China): inking continental weathering and marine C-P cycles. Global and Planetary Change 216, 103927.

Hupfer, M., Lewandowski, J., 2008. Oxygen controls the phosphorus release from lake sediments – A long-lasting paradigm in limnology. International Review of Hydrobiology 93, 415-432.

Jaisi, D.P., Blake, R.E., 2010. Tracing sources and cycling of phosphorus in Peru Margin sediments using oxygen isotopes in authigenic and detrital phosphates. Geochimica et Cosmochimica Acta 74, 3199-3212.

Jaisi, D.P., Kukkadapu, R.K., Stout, L.M., Varga, T., Blake, R.E., 2011. Biotic and abiotic pathways of phosphorus cycling in minerals and sediments: insights from oxygen isotope ratios in phosphate. Environ Sci Technol 45, 6254-6261.

Jerden, J.L., Sinha, A.K., 2006. Geochemical coupling of uranium and phosphorous in soils overlying an unmined uranium deposit: Coles Hill, Virginia. Journal of Geochemical Exploration 91, 56-70.

Jiang, G., Shi, X., Zhang, S., Wang, Y., Xiao, S., 2011. Stratigraphy and paleogeography of the Ediacaran Doushantuo Formation (ca. 635–551 Ma) in South China. Gondwana Research 19, 831-849.

Jiang, Z.-H., Zhang, H., Jaisi, D.P., Blake, R.E., Zheng, A.-R., Chen, M., Zhang, X.-G., Peng, A.-G., Lei, X.-T., Kang, K.-Q., Chen, Z.-G., 2017. The effect of sample treatments on the oxygen isotopic composition of phosphate pools in soils. Chemical Geology 474, 9–16.

Jin, C., Li, C., Algeo, T.J., O'Connell, B., Cheng, M., Shi, W., Shen, J., Planavsky, N.J., 2018. Highly heterogeneous "poikiloredox" conditions in the early Ediacaran Yangtze Sea. Precambrian Research 311, 157-166.

Joshi, S.R., Kukkadapu, R.K., Burdige, D.J., Bowden, M.E., Sparks, D.L., Jaisi, D.P., 2015. Organic matter remineralization predominates phosphorus cycling in the mid-Bay sediments in the Chesapeake Bay. Environ Sci Technol 49, 5887-5896.

Laakso, T.A., Sperling, E.A., Johnston, D.T., Knoll, A.H., 2020. Ediacaran reorganization of the marine phosphorus cycle. Proc Natl Acad Sci (U.S.A.) 117, 11961-11967.

Lécuyer, C., Amiot, R., Touzeau, A., Trotter, J., 2013. Calibration of the phosphate $\delta^{18}O$ thermometer with carbonate–water oxygen isotope fractionation equations. Chemical Geology 347, 217-226.

Lenstra, W.K., Egger, M., van Helmond, N.A.G.M., Kritzberg, E., Conley, D.J., Slomp, C.P., 2018. Large variations in iron input to an oligotrophic Baltic Sea estuary: impact on sedimentary phosphorus burial. Biogeosciences 15, 6979-6996.

Li, C., Love, G.D., Lyons, T.W., Fike, D.A., Sessions, A.L., Chu, X., 2010. A stratified redox model for the Ediacaran ocean. Science 328, 80-83.

Liang, Y., Blake, R.E., 2006. Oxygen isotope signature of P_i regeneration from organic compounds by phosphomonoesterases and photooxidation. Geochimica et Cosmochimica Acta 70, 3957-3969.

Ling, H., Jiang, S., Feng, H., Chen, Y., Chen, J., Yang, J., 2004. Oxygen isotope geochemistry of phosphorite and dolomite and palaeo-ocean temperature estimation: A case study from the Neoproterozoic Doushantuo Formation, Guizhou Province, South China. Progress in Natural Science 14, 77-84.

Liu, Z., Algeo, T.J., Brocks, J.J., van Maldegem, L.M., Gilleaudeau, G.J., Kah, L.C., Cheng, M. and Yu, W., 2025. Salinity reconstruction in Proterozoic depositional systems. Geological Society of America Bulletin 137 (1-2), 447-464.

Loyd, S.J., Corsetti, F.A., Eagle, R.A., Hagadorn, J.W., Shen, Y., Zhang, X., Bonifacie, M., Tripati, A.K., 2015. Evolution of Neoproterozoic Wonoka–Shuram Anomaly-aged carbonates: Evidence from clumped isotope paleothermometry. Precambrian Research 264, 179-191.

Luo, G., Algeo, T.J., Huang, J., Zhou, W., Wang, Y., Yang, H., Richoz, S., Xie, S., 2014. Vertical $\delta^{13}C_{org}$ gradients record changes in planktonic microbial community composition during the end-Permian mass extinction. Palaeogeography, Palaeoclimatology, Palaeoecology 396, 119-131.

Papadomanolaki, N.M., Lenstra, W.K., Wolthers, M., Slomp, C.P., 2022. Enhanced phosphorus recycling during past oceanic anoxia amplified by low rates of apatite authigenesis. Sci Adv 8, eabn2370.

Pörtner, H.O., 2010. Oxygen- and capacity-limitation of thermal tolerance: a matrix for integrating climate-related stressor effects in marine ecosystems. The Journal of Experimental Biology 213, 881-893.

Pucéat, E., Joachimski, M.M., Bouilloux, A., Monna, F., Bonin, A., Motreuil, S., Morinière, P., Hénard, S., Mourin, J., Dera, G., Quesne, D., 2010. Revised phosphate–water fractionation equation reassessing paleotemperatures derived from biogenic apatite. Earth and Planetary Science Letters 298, 135-142.

Rasmussen, B., 1996. Early-diagenetic REE-phosphate minerals (florencite, gorceixite, crandallite, and xenotime) in marine sandstones; a major sink for oceanic phosphorus. American Journal of Science 296, 601-632.

Reinhard, C.T., Planavsky, N.J., Gill, B.C., Ozaki, K., Robbins, L.J., Lyons, T.W., Fischer, W.W., Wang, C., Cole, D.B., Konhauser, K.O., 2017. Evolution of the global phosphorus cycle. Nature 541, 386-389.

Rhein, M., Rintoul, S.R., Aoki, S., Campos, E., Chambers, D., Feely, R.A., Gulev, S., Johnson, G.C., Josey, S.A., Kostianoy, A., Mauritzen, C., 2013. Observations: ocean. In: Stocke, T.F., Qin, D., Plattner, G.K., et al., editors. Climate change 2013: the physical science basis. Contribution of Working Group I to the Fifth Assessment Report of the Intergovernmental Panel on Climate Change. Cambridge: Cambridge University Press. 2013.

Robert, F., Chaussidon, M., 2006. A palaeotemperature curve for the Precambrian oceans based on silicon isotopes in cherts. Nature 443, 969-972.

Ruttenberg, K.C., Berner, R.A., 1993. Authigenic apatite formation and burial in sediments from non-upwelling, continental margin environments. Geochimica et Cosmochimica Acta 57, 991-1007.

Sahoo, S.K., Planavsky, N.J., Jiang, G., Kendall, B., Owens, J.D., Wang, X., Shi, X., Anbar, A.D., Lyons, T.W., 2016. Oceanic oxygenation events in the anoxic Ediacaran ocean. Geobiology 14, 457-468.

Sansjofre, P., Ader, M., Trindade, R.I.F., Elie, M., Lyons, J., Cartigny, P., Nogueira, A.C.R., 2011. A carbon isotope challenge to the snowball Earth. Nature 478, 93-

96.

Schwid, M.F., Xiao, S., Hiatt, E.E., Fang, Y., Nolan, M.R., 2020. Iron phosphate in the Ediacaran Doushantuo Formation of South China: A previously undocumented marine phosphate sink. Palaeogeography, Palaeoclimatology, Palaeoecology 560, 109993.

Shemesh, A., Kolodny, Y., Luz, B., 1983. Oxygen isotope variations in phosphate of biogenic apatites, II. Phosphorite rocks. Earth and Planetary Science Letters 64, 405-416.

Smith, A.C., Pfahler, V., Tamburini, F., Blackwell, M.S.A., Granger, S.J., 2021. A review of phosphate oxygen isotope values in global bedrocks: Characterising a critical endmember to the soil phosphorus system. Journal of Plant Nutrition and Soil Science 184, 25-34.

Sperling, E.A., Wolock, C.J., Morgan, A.S., Gill, B.C., Kunzmann, M., Halverson, G.P., Macdonald, F.A., Knoll, A.H., Johnston, D.T., 2015. Statistical analysis of iron geochemical data suggests limited late Proterozoic oxygenation. Nature 523, 451-454.

Sun, Y., Amelung, W., Wu, B., Haneklaus, S., Maekawa, M., Lücke, A., Schnug, E., Bol, R., 2020. 'Co-evolution' of uranium concentration and oxygen stable isotope in phosphate rocks. Applied Geochemistry 114, 104476.

Vuillemin, A., Ariztegui, D., De Coninck, A.S., Lücke, A., Mayr, C., Schubert, C.J., The, P.S.T., 2013. Origin and significance of diagenetic concretions in sediments of Laguna Potrok Aike, southern Argentina. Journal of Paleolimnology 50, 275-291.

Wang, W., Guan, C., Zhou, C., Peng, Y., Pratt, L.M., Chen, X., Chen, L., Chen, Z., Yuan, X., Xiao, S., 2017. Integrated carbon, sulfur, and nitrogen isotope chemostratigraphy of the Ediacaran Lantian Formation in South China: Spatial gradient, ocean redox oscillation, and fossil distribution. Geobiology 15, 552-571.

Wei, W., Yu, W., Du, Y., Algeo, T.J., Li, Z., Cheng, M., Wang, P., Zhang, J., Robbins, L.J., Konhauser, K., 2024. A new salinity-based model for Cryogenian Mn-carbonate deposits. Precambrian Research 403, 107309.

Xiao, S., Muscente, A.D., Chen, L., Zhou, C., Schiffbauer, J.D., Wood, A.D., Polys, N.F., Yuan, X., 2014. The Weng'an biota and the Ediacaran radiation of multicellular eukaryotes. National Science Review 1, 498-520.

Yang, H., Xiao, J., Xia, Y., Xie, Z., Tan, Q., Xu, J., He, S., Wu, S., Liu, X., Gong, X., 2021. Phosphorite generative processes around the Precambrian-Cambrian boundary in South China: An integrated study of Mo and phosphate O isotopic compositions. Geoscience Frontiers 12, 101187.

Ye, Y., Wu, C., Zhai, L., An, Z., 2017. Pyrite morphology and episodic euxinia of the Ediacaran Doushantuo Formation in South China. Science China Earth Sciences

60, 102-113.

Yu, W., Algeo, T.J., Zhou, Q., Wei, W., Yang, M., Li, F., Du, Y., Pan, W., Wang, P., 2022. Evaluation of alkalinity sources to Cryogenian cap carbonates, and implications for cap carbonate formation models. Global and Planetary Change 217, 103949.

Yuan, H., Li, Q., Kukkadapu, R.K., Liu, E., Yu, J., Fang, H., Li, H., Jaisi, D.P., 2019. Identifying sources and cycling of phosphorus in the sediment of a shallow freshwater lake in China using phosphate oxygen isotopes. Science of The Total Environment 676, 823-833.

Yuan, X., Chen, Z., Xiao, S., Zhou, C., Hua, H., 2011. An early Ediacaran assemblage of macroscopic and morphologically differentiated eukaryotes. Nature 470, 390-393.

Zhang, S., Li, H., Jiang, G., Evans, D.A.D., Dong, J., Wu, H., Yang, T., Liu, P., Xiao, Q., 2015. New paleomagnetic results from the Ediacaran Doushantuo Formation in South China and their paleogeographic implications. Precambrian Research 259, 130-142.

Figure 1. A. Simplified paleogeographic map of South China during the Ediacaran Period, highlighting the study area, early biotas, and giant phosphorite deposits. B. Stratigraphic columns of the two investigated sections (Wuhe and Yinjiang), showing estimated redox conditions (Han and Fan, 2015; Sahoo et al., 2016; Ye et al., 2017) and potential correlation withs the Weng'an and Lantian Biotas.

Figure 2. SEM images of major phosphate minerals in selected samples from the Wuhe and Yinjiang sections.

Figure 3. Stratigraphic curves of TOC/P ratios, $\delta^{13}C_{org,}$ and $\delta^{18}O_P$ values from the Wuhe (A) and Yinjiang (B) sections, highlighting similarities in the three investigated proxies between the two sections. In (A), the purple shaded areas represent euxinic intervals characterized by abnormally negative $\delta^{13}C_{org}$ values (< –32‰) and predominantly higher TOC/P ratios compared to the Redfield ratio (106), marked by black dashed lines. Blue shaded areas (A, B) represent intervals with $\delta^{18}O_P$ values similar to those of modern seawater.

Figure 4. The TOC/P ratios are plotted against $\delta^{13}C_{org}$ (A) and $\delta^{18}O_P$ values (B) to investigate patterns of phosphorus recycling and oxygen isotope fractionations in the Nanhua Basin. The data suggest generally weak phosphorus recycling and complex oxygen isotope fractionation across the study area. Shelf and basin data in (A) are cited from Fang et al. (2019).

Figure 5. Surface seawater paleotemperatures during the early to middle Ediacaran were calculated following the equation from Lécuyer et al. (2013). These calculations reveal distinct environmental differences between the Lantian Biota (~602 ± 7 Ma) and the Weng’an Biota (~587 Ma). The Lantian Biota developed in a deep-water environment with lower oxygen levels and a relatively cold, narrow temperature range (~7–8 ± 2 °C, see **Appendix A**). In contrast, the Weng’an Biota inhabited a high O_2 shallow-water outer shelf environment, where seawater temperatures were notably higher and varied within a broader range (16–30 °C). These differences underscore the environmental diversity of the Ediacaran period and its influence on biotic distribution.

Declaration of interests

☒ The authors declare that they have no known competing financial interests or personal relationships that could have appeared to influence the work reported in this paper.

☐ The authors declare the following financial interests/personal relationships which may be considered as potential competing interests:

Highlights

- First report of $\delta^{18}O_P$ for Ediacaran marine siliciclastic rocks
- Samples dominated by Fe/Al-phosphate can preserve original $\delta^{18}O_P$ values
- The Doushantuo Formation records modern seawater-like $\delta^{18}O_P$ values
- These $\delta^{18}O_P$ yield a seawater temperature range for the Ediacaran similar to modern
- Cool temperatures may have facilitated evolution of early multicellular eukaryotes

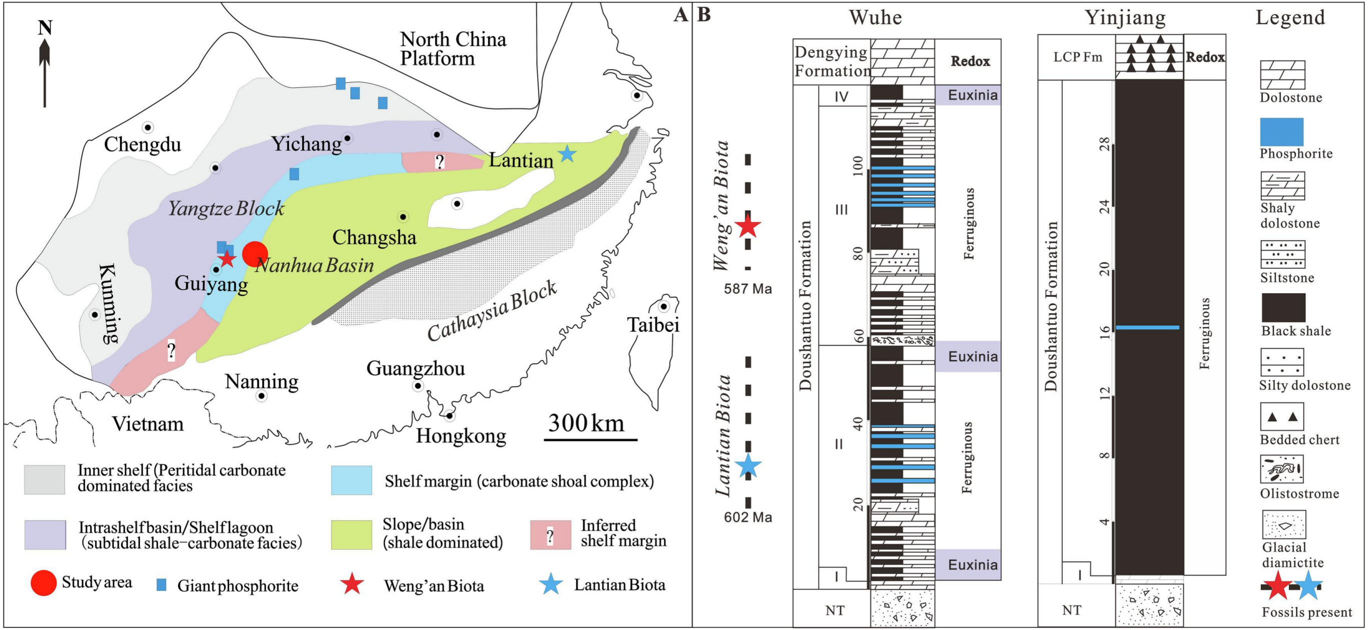

A
N
North China Platform
Chengdu
Yichang
Lantian
Yangtze Block
Changsha
Guiyang
Nanhua Basin
Kunming
Cathaysia Block
Taibei
Nanning
Guangzhou
Vietnam
Hongkong
300 km
Inner shelf (Peritidal carbonate dominated facies
Shelf margin (carbonate shoal complex)
Intrashelfbasin/Shelflagoon (subtidal shale−carbonate facies)
Slope/basin (shale dominated)
Inferred shelf margin
Study area
Giant phosphorite
Weng'an Biota
Lantian Biota
B
Wuhe
Yinjiang
Legend
Dengying Formation
Redox
Euxinia
Ferruginous
Doushantuo Formation
IV
III
II
I
NT
Weng'an Biota
587 Ma
Lantian Biota
602 Ma
LCP Fm
Dolostone
Phosphorite
Shaly dolostone
Siltstone
Black shale
Silty dolostone
Bedded chert
Olistostrome
Glacial diamictite
Fossils present

Figure 1

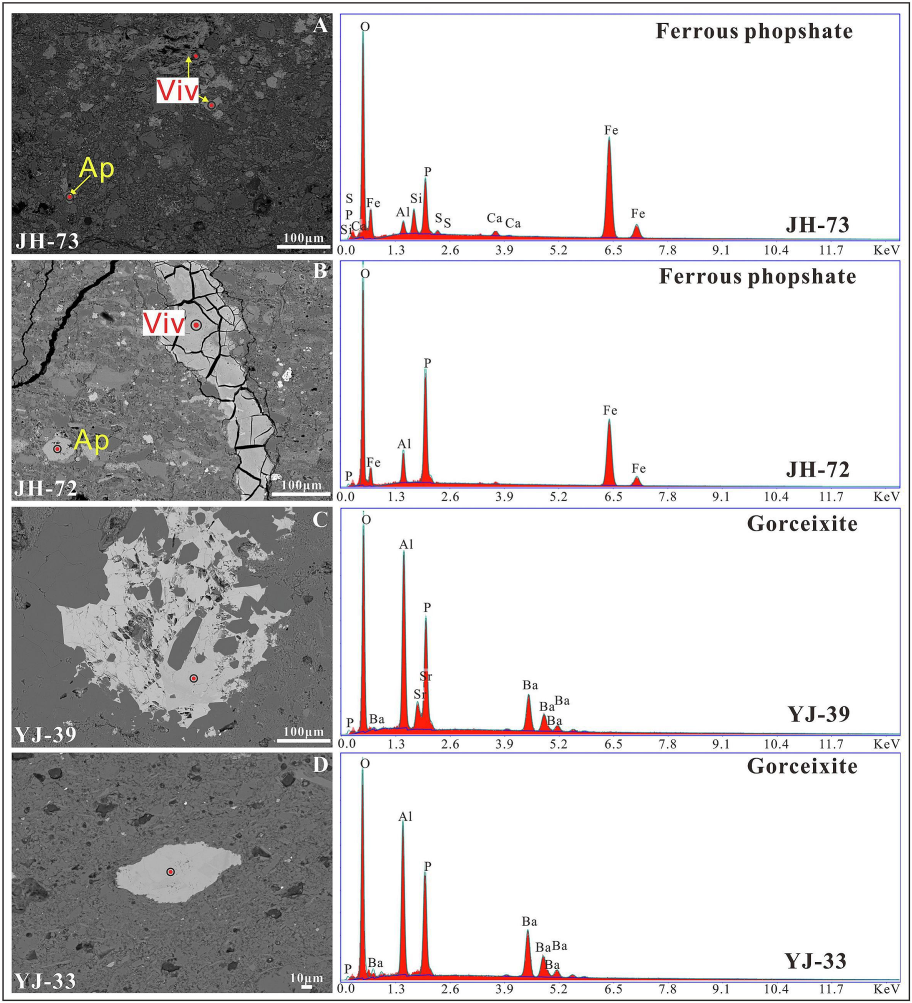
A
Viv
Ap
JH-73
100μm
Ferrous phopshate
O
Fe
P
Si
Al
S
Ca
JH-73
0.0
1.3
2.6
3.9
5.2
6.5
7.8
9.1
10.4
11.7
KeV
B
Viv
Ap
JH-72
100μm
Ferrous phopshate
JH-72
C
YJ-39
100μm
Gorceixite
Sr
Ba
YJ-39
D
YJ-33
10μm
Gorceixite
YJ-33

Figure 2

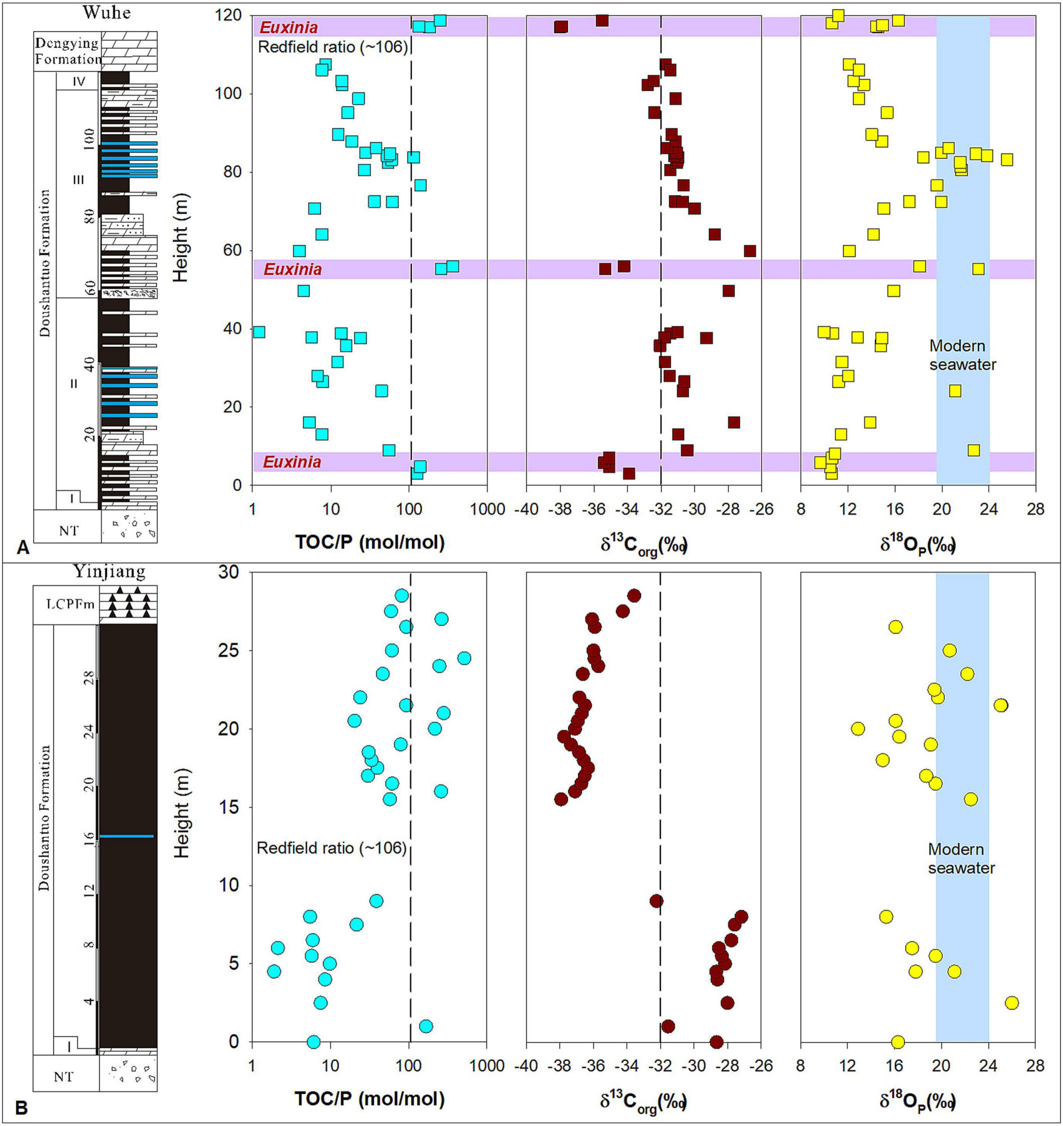

Wuhe
Dengying Formation
Doushantuo Formation
IV
III
II
I
NT
Euxinia
Redfield ratio (~106)
Height (m)
TOC/P (mol/mol)
$\delta^{13}C_{org}$(‰)
$\delta^{18}O_p$(‰)
Modern seawater
A
Yinjiang
LCPFm
Doushantuo Formation
I
NT
Redfield ratio (~106)
Height (m)
TOC/P (mol/mol)
$\delta^{13}C_{org}$(‰)
$\delta^{18}O_p$(‰)
Modern seawater
B

Figure 3

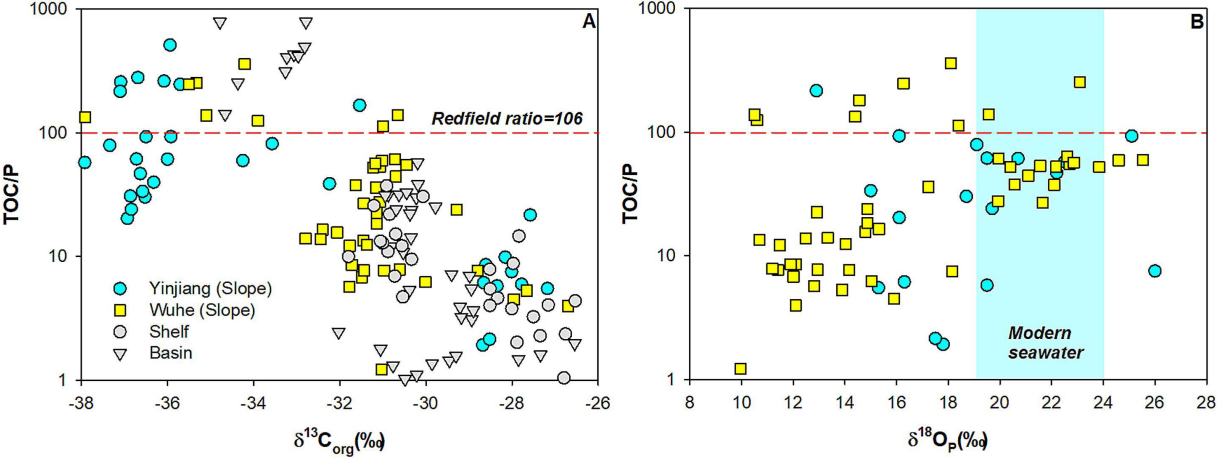

A
Redfield ratio=106
TOC/P
Yinjiang (Slope)
Wuhe (Slope)
Shelf
Basin
1000
100
10
1
-38
-36
-34
-32
-30
-28
-26
δ13Corg(‰)
B
Modern seawater
δ18OP(‰)
8
10
12
14
16
18
20
22
24
26
28

Figure 4

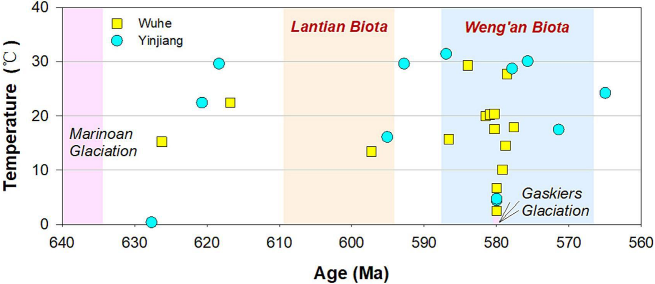

Wuhe
Yinjiang
Lantian Biota
Weng'an Biota
Marinoan Glaciation
Gaskiers Glaciation
Temperature (℃)
Age (Ma)
0
10
20
30
40
640
630
620
610
600
590
580
570
560

Figure 5